Physics and Imaging in Radiation Oncology 11 (2019) 82–87

Contents lists available at ScienceDirect

Physics and Imaging in Radiation Oncology

journal homepage: www.elsevier.com/locate/phro

Original Research Article

Effects of age-related breathing characteristics on the performance of four-dimensional magnetic resonance imaging reconstructed by prospective gating for radiation therapy planning

Jinsoo Uh[a,*], Mo Kadbi[b], Chia-ho Hua[a]

[a] Department of Radiation Oncology, St. Jude Children's Research Hospital, Memphis, TN, USA
[b] Philips Healthcare, Gainesville, FL, USA

ARTICLE INFO

Keywords:
Four-dimensional magnetic resonance imaging (4D MRI)
Pediatric patients
Prospective gating
Retrospective sorting
Respiration characteristics
Breathing irregularity

ABSTRACT

Background and purpose: Four-dimensional magnetic resonance imaging (4D MRI) has advanced recently by incorporating prospective gating, but its performance on pediatric populations has not been investigated. This study aimed to determine the age-related performance of prospective gating, as compared with retrospective sorting.

Materials and methods: Prospectively gated 4D MRI scans were acquired on a motion phantom driven by real respiratory waveforms obtained from 23 pediatric and young adult patients (aged 5–24 years). The correlations between patient-specific breathing characteristics and the performance of 4D MRI were comparatively evaluated against retrospective sorting for the same scan time. For six patients who underwent both 4D MRI and 4D CT, the internal target volumes (ITVs) determined by the two modalities were compared.

Results: Longer scan time and greater sorting error were most highly correlated ($P < 0.001$) with breathing irregularity and extent of diaphragm motion, but age was not a strong covariate because of interindividual variation. Prospective gating was more accurate than retrospective sorting except for those patients with severe breathing irregularity (peak-to-peak coefficient of variation > 30%). The ITVs of 4D MRI and 4D CT were comparable (Dice similarity: > 90%) unless the breathing characteristics changed between the two imaging sessions.

Conclusions: For most patients analyzed in this study, prospective gating provided more accurate 4D MRI (95th percentile of deviation: < 1.5 mm) than did retrospective sorting within a clinically feasible scan time (median: 5.9 min). The 4D MRI tended to take longer and to give larger sorting errors with deeper and irregular breathers.

1. Introduction

Four-dimensional magnetic resonance imaging (4D MRI) offers unique advantages for visualizing moving soft-tissue tumors to plan radiation treatment. Many recently developed 4D MRI methods are based on radial 3D gradient-echo sequences [1–4], which are advantageous for achieving high spatiotemporal resolution, reducing sorting artifacts, and deriving a robust respiratory surrogate signal. However, these methods have not been widely adopted in clinical practice because the iterative image reconstruction requires extensive computation with unconventional software or hardware that is not commonly available in clinical environments. In addition, the image contrast, which is typically T1 weighted, is often suboptimal for delineating tumor volumes.

As an alternative, 4D MRI can be performed using 2D spin-echo sequences, which provide a favorable T2-weighted image contrast and facilitate implementation on clinical scanners. Recently, an important advance has been made in such methods by incorporating prospective gating [5–9], which improves the scanning efficiency and binning accuracy. A previous study showed that the performance of prospective gating is subject to the respiration characteristics of the patient [7], but that study did not include pediatric patients and the number and diversity of the breathing characteristics were somewhat limited. Reports of previous 4D MRI studies on pediatric patients are scarce [10], and no such studies using prospective gating have been reported. Challenges in 4D MRI that are particularly associated with pediatric patients include the diverse respiratory characteristics of these patients and varied ability to tolerate a prolonged scan time, which need to be understood for this advanced imaging method to be applied clinically.

The primary aim of this study was to investigate the effect of age-

* Corresponding author at: Department of Radiation Oncology, St. Jude Children's Research Hospital, 262 Danny Thomas Place, Memphis, TN 38105, USA.
E-mail address: jinsoo.uh@stjude.org (J. Uh).

https://doi.org/10.1016/j.phro.2019.09.004
Received 11 July 2019; Received in revised form 4 September 2019; Accepted 10 September 2019
2405-6316/ © 2019 The Authors. Published by Elsevier B.V. on behalf of European Society of Radiotherapy & Oncology. This is an open access article under the CC BY-NC-ND license (http://creativecommons.org/licenses/BY-NC-ND/4.0/).

related breathing characteristics of pediatric patients on the performance of the prospective gating algorithm. Furthermore, we compared the prospectively gated 4D MRI with retrospectively sorted 4D MRI, as well as with 4D CT. Three underlying hypotheses were examined in this study: (1) that the performance of the prospective gating algorithm was dependent on the breathing characteristics of pediatric patients; (2) that prospective gating would perform better than retrospective sorting; and (3) that 4D MRI could be an alternative to 4D CT for determining target margins in pediatric treatment planning.

2. Materials & methods

2.1. Overview of the method

This institutional review board–approved study was composed of two parts: a phantom experiment and a patient study. The purpose of the phantom experiment was to investigate the effect of breathing characteristics on the prospective gating as compared with retrospective sorting. The use of a phantom facilitated specifying the respiratory motion for a given imaging method and parameter set. It also enabled the adoption of diverse respiratory waveforms from previous clinical 4D CT scans. The patient study was primarily designed to quantitatively compare target margins determined by prospectively gated 4D MRI and 4D CT, but the data were also used to qualitatively evaluate the image quality.

2.2. Phantom experiment

2.2.1. Data acquisition

We have developed an in-house 4D MRI phantom that can be driven by real respiratory waveforms derived from humans. Supplementary material A provides details of the phantom, along with a validation. A comparison of phantom and in vivo 4D MRIs is presented in Supplementary material B. The respiratory waveforms (henceforth referred to as the "feed signals") employed to drive the motion phantom were obtained from clinical scans acquired for radiation therapy planning. They comprised navigator radiofrequency (RF) signals of prospectively gated 4D MRI scans (n = 5) and pneumatic bellows belt signals used for reconstructing 4D CT (n = 18). The demographics associated with the feed signals and their individual plots are provided in Table 1 and Supplementary material C, respectively.

All 4D MRI scans were performed on a 1.5-T scanner (Ingenia; Philips Healthcare, Gainesville, FL). Multi-slice 2D turbo spin-echo images at 10 respiratory phases were acquired by the prospective gating algorithm, which has been described in detail in previous publications [5–8] and is briefly described in Supplementary material D. The imaging parameters were as follows: image orientation: coronal; field of view (FOV): 300 × 300 mm^2; in-plane resolution: 1.5 × 1.5 mm^2; slice thickness: 4 mm; number of slices: 40; minimum repetition time (TR): 4 s; echo time (TE): 80 ms; half-scan factor: 0.6; echo train length: 61; shot length: 431 ms.

For comparison purposes, the phantom experiments were repeated with a retrospective sorting method, using the same feed signals. The imaging parameters were mostly the same as those for the prospective gating except that the entire image volume was repeatedly acquired with a fixed time gap, TR, of 4.5 s. The scan time was made the same as that for the prospective gating to enable a fair comparison. Once the image slices were acquired, the amplitude of the surrogate signal at each slice acquisition was determined using information in the log files, and the inhalation and exhalation phases were distinguished by the sign of the amplitude changes. The slices exhibiting the amplitudes closest to each triggering level of the prospective gating were then assembled to produce a 3D volume for each phase.

2.2.2. Data processing

The respiratory surrogate signal recorded by the scanner was collected from the log files after each scan to quantify breathing characteristics and compare the performance of the prospective gating and retrospective sorting algorithms. The end-inhalation and end-exhalation points in the respiratory surrogate signal were identified by an automatic algorithm [11]. The mean period per breath was calculated from those points to give the respiration rate. The coefficient of variation (CV) of the peak-to-peak amplitude was calculated to quantify the irregularity of breathing.

The log files also provided the time points of each slice acquisition and the corresponding signal amplitudes, from which we calculated the sorting error as defined in the following. The retrospective sorting redundantly samples at a fixed rate and selects optimal image slices out of those at virtually random respiratory phases. Therefore, it is not guaranteed to find sufficiently coherent images, which results in stitching artifacts (also known as staircase artifacts) in the reconstructed image volumes. In contrast, prospective gating triggers image acquisition only when the surrogate signal approaches a given amplitude level. However, it is not exempt from stitching artifacts either, because of the triggering tolerance. To quantify the artifact arising from such imperfect image sorting or gating, we defined the sorting error by

$$\varepsilon_{s,p} = a_{s,p} - \frac{\sum_{i=1}^{N_s} a_{i,p}}{N_s},$$

where $a_{s,p}$ is the amplitude of a slice at location s (=1, 2, ...,N_s) and phase p (=1, 2, ...,N_p), N_s is the number of slices, and N_p is the number of phases. We calculated the mean error over all slices in all volumes, $\sum_{s=1}^{N_s}\sum_{p=1}^{N_p} \varepsilon_{s,p}/(N_s N_p)$, as well as its 95th percentile and the maximum value.

2.2.3. Statistical analysis and comparison

We first evaluated the age-dependent variation in the breathing characteristics (respiration rate, motion amplitude, and breathing irregularity) and then the impact of the breathing characteristics on the performance of 4D MRI (scan time and mean sorting error) by calculating Pearson correlation coefficients and *P*-values. The prospective gating and retrospective sorting were compared in terms of the sorting error and the associations with breathing characteristics. All comparisons and statistical analyses used in-house MATLAB (Math Works, Natick, MA) scripts.

2.3. Patient study

2.3.1. Data acquisition

Among the 23 patients whose respiratory data were used in the phantom experiment, those who underwent 4D CT and prospectively gated 4D MRI scans on the same day (n = 6) were included in the patient study. The clinical 4D CT was acquired on a Brilliance Big Bore CT scanner or a Vereos PET/CT system (Philips Healthcare, Cleveland, OH) with 120 kVp, 0.04 spiral pitch factor, 0.625-mm collimation, a 50-cm FOV, and slice thickness of 2–3 mm. The number of respiratory phases was 10, and conventional phase-based binning was used for image reconstruction. The scanner and imaging parameters of the clinical 4D MRI were the same as those of the phantom experiment except for the patient-specific parameters shown in Table 2.

All patients were allowed to breathe freely during both 4D imaging scans. Patients younger than 7 years underwent general anesthesia with intravenously administered propofol (150–270 μg/kg/min). They breathed on their own, with supplementary oxygen being delivered via a nasal cannula or facial mask.

2.3.2. Data processing

The planning CT, clinical target volume (CTV), and all 4D images (i.e., from 4D MRI and 4D CT) were transferred to MIM software (MIM Software, Cleveland, OH). Each 4D dataset was registered to the

Table 1
Information on the respiratory signals used for the phantom experiments and the performance results.

Patient	Sex	Age	Source of respiratory waveform	General anesthesia*	Resp. rate (breaths/min)	Diaph. motion (mm)	Breathing irregularity† (%)	Scan time (min)	Deviation (mm)					
									Mean		95th percentile		Max	
									Pro.	Retro.	Pro.	Retro.	Pro.	Retro.
1	F	5	4D CT	Yes	28.7	5.2	7.4	4.9	0.18	0.33	0.50	1.02	1.21	1.94
2	M	5	4D MRI	Yes	16.8	12.5	12.6	6.1	0.44	1.00	1.21	3.43	2.12	6.97
3	M	5	4D CT	Yes	22.1	4.4	8.9	4.6	0.15	0.29	0.40	0.91	0.98	1.67
4	F	6	4D CT	Yes	15.6	6.3	13.2	6.5	0.20	0.30	0.49	0.93	1.08	1.86
5	M	6	4D CT	Yes	16.6	6.5	7.3	6.1	0.18	0.36	0.46	1.13	0.91	2.19
6	M	12	4D CT	No	20.6	14.8	9.7	5.3	0.41	0.80	1.07	2.48	2.27	4.86
7	F	12	4D MRI	No	16.9	7.5	35.8	6.6	0.34	0.68	0.89	2.40	3.10	4.61
8	F	13	4D CT	No	18.4	10.5	5.5	5.9	0.34	0.92	0.85	3.13	2.46	6.81
9	F	13	4D MRI	No	25.9	6.7	29.4	4.3	0.34	0.57	0.95	1.79	2.32	4.65
10	F	15	4D CT	No	10.1	17.6	22.6	7.7	0.54	0.86	1.35	2.66	3.77	5.33
11	M	15	4D CT	No	20.5	12.2	13.9	4.7	0.41	0.83	1.07	2.44	2.08	5.27
12	M	15	4D CT	No	14.7	9.3	28.7	6.9	0.44	0.52	1.19	1.49	3.57	3.64
13	F	17	4D CT	No	8.5	16.3	31.6	15.1	0.63	0.55	1.47	1.79	3.44	3.89
14	F	17	4D MRI	No	17.7	6.6	20.5	5.8	0.27	0.57	0.73	2.03	1.32	3.48
15	F	17	4D CT	No	10.9	8.5	22.8	5.9	0.33	0.51	0.89	1.46	1.63	2.41
16	M	17	4D MRI	No	6.1	30.2	26.3	7.7	1.62	2.22	4.56	7.13	8.43	12.93
17	F	17	4D CT	No	21.0	4.3	21.2	5.9	0.18	0.34	0.48	1.00	0.81	2.40
18	M	18	4D CT	No	12.2	8.0	7.2	5.5	0.25	0.55	0.66	1.94	3.05	3.62
19	M	19	4D CT	No	13.1	17.1	16.8	5.9	0.53	0.97	1.22	2.60	2.81	7.28
20	M	20	4D CT	No	12.6	13.8	11.4	6.4	0.33	0.76	0.92	2.65	2.12	6.01
21	F	20	4D CT	No	16.9	10.0	27.2	7.4	0.34	0.61	0.90	1.90	1.56	3.92
22	F	20	4D CT	No	10.6	11.6	13.5	5.2	0.35	0.82	0.82	2.40	1.33	5.96
23	M	24	4D CT	No	6.7	18.0	52.4	12.7	1.27	1.12	3.35	3.86	14.31	8.85
Min.		5			6.1	4.3	5.5	4.3	0.15	0.29	0.40	0.91	0.81	1.67
Max.		24			28.7	30.2	52.4	15.1	1.62	2.22	4.56	7.13	14.31	12.93
Median		15			16.6	10.0	16.8	5.9	0.34	0.61	0.90	2.03	2.12	4.61

Abbreviations: Diaph. motion: peak-to-peak diaphragm motion; F: female; M: male; Max.: maximum; Min.: minimum, Pro.: prospective gating; Resp.: respiration, Retro.: retrospective sorting.

* Patients younger than 7 years underwent general anesthesia with intravenously administered propofol (150–270 μg/kg/min).

† Breathing irregularity was quantified by the coefficient of variation of the peak-to-peak amplitude in the respiratory signal.

planning CT based on spine regions in the end-exhalation phase. Deformation fields across different image volumes were automatically derived by MIM software and applied to the CTV. The union of the resultant CTVs at 10 respiratory phases yielded the ITV.

2.3.3. Statistical analysis and comparison

The ITVs derived by 4D CT and 4D MRI, as well as the CTV in cubic centimeters, were recorded from the display of the MIM software. A Boolean operation tool in the software was used to calculate the overlapped volume of the ITVs from the two modalities. The Dice similarity coefficient was calculated as follows:

$$\text{Dice coefficient}\ (\%) = \frac{2 \times ITV_{overlap}}{ITV_{4DCT} + ITV_{4DMRI}}$$

3. Results

3.1. Variation in breathing characteristics

The respiration rates of the patients ranged from 6.1 to 28.7 breaths/min (Table 1). As expected, older patients breathed more slowly than did younger patients ($R = 0.59$, $P = 0.003$). The diaphragm motion (range: 4.3–30.2 mm) tended to be greater in the older patients ($R = 0.42$, $P = 0.046$), but interindividual variation was apparent. For instance, the motion in the five 17-year-old patients (Patients 13–17) ranged from 4.3 mm to 30.2 mm. The breathing irregularity quantified by amplitude variation also showed a correlation with age ($R = 0.51$, $P = 0.01$) and interindividual variation.

3.2. Impact of breathing characteristics on 4D MRI performance

The scan time for the prospective gating method ranged from 4.3 min to 15.1 min (Table 1), but it was mostly less than 8 min except for the two patients (Patients 13 and 23) with marked breathing irregularities (CV > 30%). The mean deviation was submillimetric, and the 95th percentile was smaller than the in-plane resolution (1.5 mm) for all patients with diaphragm motion and irregularity less than 20 mm and 30%, respectively (Patients 16 and 23 did not meet these conditions).

The phantom experiments revealed that longer scan time correlated with slower respiration rate, greater internal organ motion, and irregular breathing (Fig. 1), among which breathing irregularity showed the highest correlation with the scan time ($R = 0.65$, $P < 0.001$). In contrast, the age of the patient did not correlate significantly with the scan time ($R = 0.37$, $P = 0.08$). The sorting error, in terms of the mean deviation, correlated most significantly with the diaphragm motion ($R = 0.89$, $P < 0.001$), as demonstrated in Fig. 2(A and B).

3.3. Comparison of prospective and retrospective sorting

Interestingly, the accuracy of retrospective sorting did not correlate with breathing irregularity ($R = 0.25$, $P = 0.25$). This is because the retrospective sorting was allowed to take as long as prospective gating in cases of irregular breathing, which improved the accuracy. However, the accuracy of retrospective sorting exceeded that of prospective gating only for those abovementioned patients with marked irregularities (Table 1). Fig. 3 demonstrates that the sorting error tended to be larger near end-inhalation (phase 5) than near end-exhalation (phase 1 or 10) with retrospective sorting, whereas the error was more or less uniformly distributed across all phases with prospective gating.

Table 2
Patient-specific clinical parameters and comparison of 4D MRI with 4D CT.

Patient	Diagnosis	Treatment site	4D MRI parameters			
			Orientation	FOV (mm^2)	No. of slices	Resolution (mm^3)
2	Neuroblastoma	Chest apex	Coronal	300 × 300	44	1.5 × 1.5 × 4.0
4	Neuroblastoma	Adrenal	Transverse	300 × 300	42	1.8 × 1.8 × 4.0
7	Rhabdomyosarcoma	Porta hepatis	Coronal	335 × 307	40	1.5 × 1.5 × 5.0
9	Rhabdomyosarcoma	Chest wall	Sagittal	300 × 220	30	2.0 × 2.0 × 6.0
14	Rhabdomyosarcoma	Mediastinum	Coronal	291 × 361	46	1.5 × 1.5 × 5.0
16	Hodgkin lymphoma	Mediastinum	Coronal	350 × 344	52	1.5 × 1.5 × 4.0

Patient	Respiration rate (breaths/min)		Breathing irregularity* (%)		Scan time (min)		CTV (cc)	ITV (cc)		Dice similarity (%)
	4D MRI	4D CT	4D MRI	4D CT	4D MRI	4D CT		4D MRI	4D CT	
2	16.8	18.1	12.6	7.7	5.6	0.8	191	195	209	95
4	16.0	15.6	8.7	13.2	9.0	1.4	105	116	114	95
7	16.9	15.2	35.8	33.1	7.2	1.4	101	123	132	92
9	25.9	18.4	29.4	33.2	2.7	1.2	15	17	24	82
14	17.7	17.4	20.5	32.0	6.7	1.8	68	94	85	83
16	6.1	15.6	26.3	48.5	8.5	1.6	120	174	146	88

Abbreviations: 4D CT: four-dimensional computed tomography; 4D MRI: four-dimensional magnetic resonance imaging; CTV: clinical target volume; FOV: field of view; ITV: internal target volume.

* Breathing irregularity was quantified by the coefficient of variation of the peak-to-peak amplitude in the respiratory signal.

3.4. Comparison of ITVs derived from 4D MRI and 4D CT

The respiration rates and the irregularity were not always similar at the times of the 4D MRI and 4D CT scans, implying that there was temporal variation in the breathing characteristics (Table 2). The scans of Patient 9 were affected by coughing and voluntary motion. The 4D MRI of this patient was repeated because of severe motion artifacts, which led to the FOV and resolution being compromised to reduce the scan time as much as possible (to 2.7 min). Patient 14 showed intermittent deep breathing, which resulted in a large difference in breathing irregularity for the 4D MRI and 4D CT (CVs of 21% and 32%, respectively). For Patient 16, the RF navigator of 4D MRI could often not detect respiratory phases for more than 10 s at a time, possibly because of very shallow or slow breathing (see the waveform in Supplementary material C). Consequently, the calculated mean respiration rate (6.1 breaths/min) was considerably lower than that for the 4D CT (15.6 breaths/min).

The expansion in volume from the CTV to the ITV was 2%–46% and 9%–63% with 4D MRI and 4D CT, respectively (Table 2). The Dice similarity was 92%–95% for the three youngest patients, who showed relatively similar breathing characteristics with the two imaging modalities. Reduced dice similarities (82%–88%) were found in the other patients, which partly reflected the aforementioned confounding factors and temporal variation in breathing characteristics.

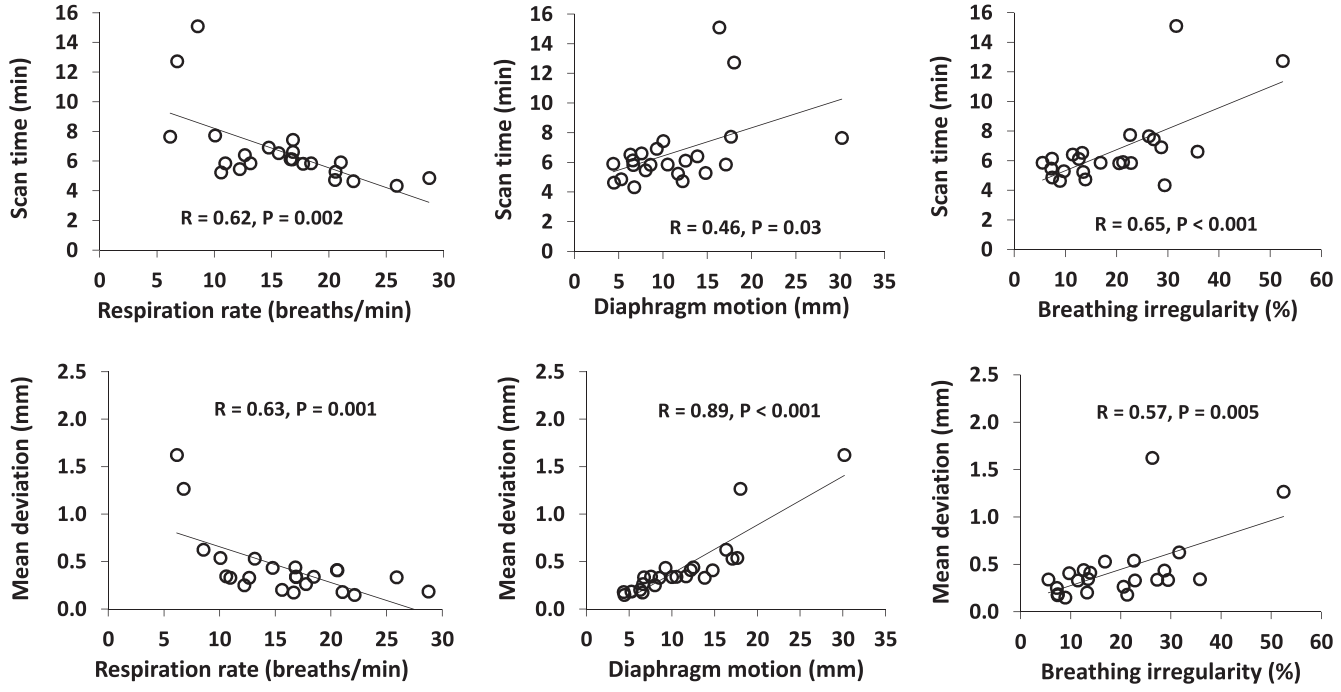

Fig. 1. Correlations between respiratory characteristics (rate, amplitude, and irregularity) and the performance of prospectively gated 4D MRI (scan time and mean deviation). Breathing irregularity indicates the coefficient of variation of the peak-to-peak amplitude in the respiratory waveforms.

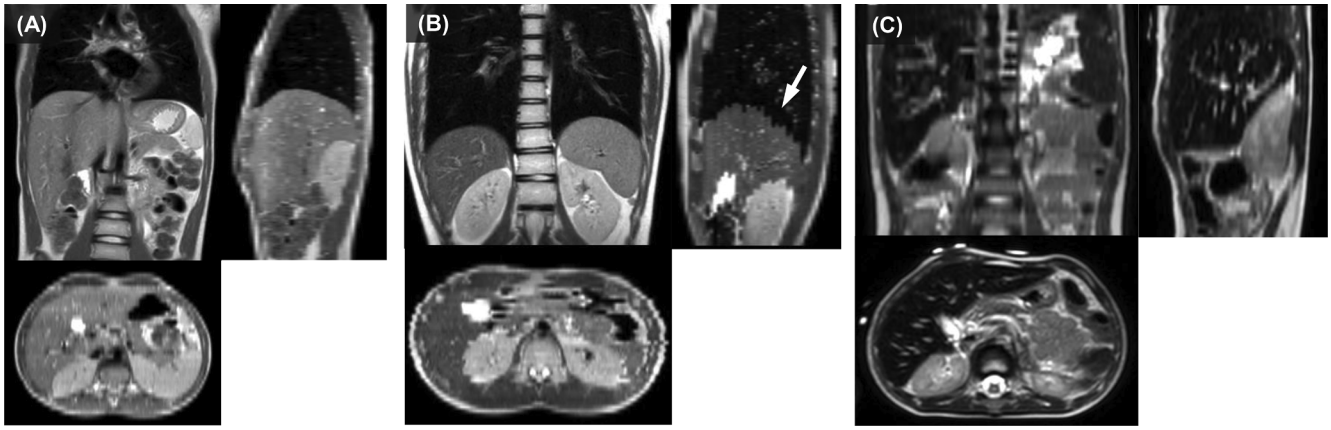

Fig. 2. Examples of 4D MRI scans prospectively gated from coronal (A and B) or transverse (C) image slices. Images of a patient with relatively small organ motion (Patient 7; peak-to-peak diaphragm motion: 7.5 mm) (A) showed no apparent sorting artifacts, whereas images of another patient with greater motion (Patient 16; peak-to-peak diaphragm motion: 30.2 mm) (B) did show artifacts. The signal from liver was dark for a patient (Patient 4) who had received multiple blood transfusions, possibly because of iron overload (C).

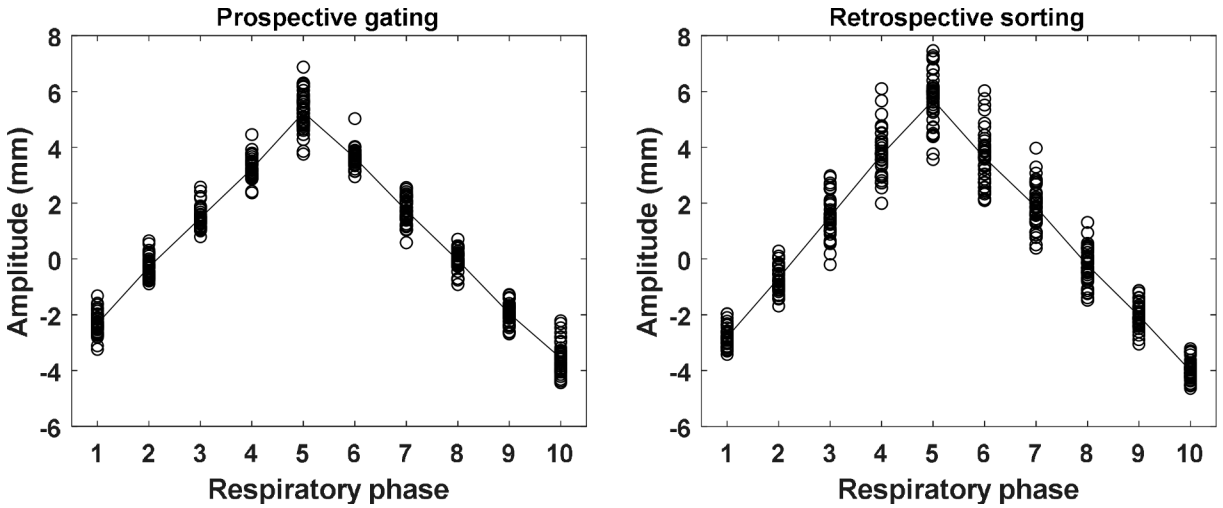

Fig. 3. Comparison of sorting accuracy with prospective gating and retrospective sorting for a representative case (Patient 11). The solid line indicates the mean displacement at each phase, the deviation from which was calculated to evaluate the sorting error.

4. Discussion

The phantom experiment showed that the prospectively gated 4D MRI took less than 8 min for the tested imaging parameters and that the stitching artifact (i.e., sorting error) was submillimetric for most cases with breathing irregularity less than a CV of 30% and diaphragm motion of less than 20 mm. These findings can be translated to the triggering-associated performance of clinical 4D MRI on patients. Because the prospective triggering algorithm relies only on the respiratory surrogate signal, its performance in patient scans would not differ from that in the phantom experiment in which real respiratory waveforms were implemented. However, the phantom images of a liquid bottle were not appropriate for evaluating resolution and contrast. The discussions regarding such image quality are based on patient 4D MRI, as described below.

The prospective gating gave smaller errors than did retrospective sorting (Table 1 and Fig. 3) for most cases in the phantom experiments. With retrospective sorting, the error increased near end-inhalation, in which the motion is faster and the fixed sampling rate reduces the chances of finding coherent images. The prospective gating method does not have this issue, because the triggering is based on the signal amplitude instead of time. However, the reconstructed image volumes by such amplitude-based binning may not be suitable for calculating the 4D dose [12] because they do not represent the same amount of time. An alternative method would be amplitude binning with even statistics [13,14], which would account for the timing of the acquired images while retaining the advantages of amplitude binning.

A rigorous comparison between 4D MRI and 4D CT was challenging because of the changes in breathing characteristics and other confounding factors, including voluntary motion and uncertainties in the image registration. The significant difference in scan time with the two imaging modalities (2.7–9.0 min for 4D MRI versus 0.8–1.8 min for 4D CT) might also have contributed to the discrepancies. The comparison suggested that there were uncertainties in the organ motion assessed by a single 4D imaging session and that frequent monitoring throughout the treatment course is warranted; 4D MRI is advantageous for this purpose owing to the absence of ionizing radiation. In our clinical practice, the ITV is determined by visual inspection and manual delineation, rather than by the automatic process involving image deformation, and all available 4D images are used in the treatment planning.

The resolution and T2-weighted image contrast of the patient 4D MRI were favorable for treatment planning. However, an inherent limitation of such 2D slice–based 4D MRI is the coarse through-plane resolution (4–6 mm), which needs to be considered when selecting the image orientation. This limitation can be compensated for by multiple

imaging of the patient in different orientations, although the total scan time will be multiplied as a result. Separate sets of 4D MRIs in different orientations would be useful in treatment planning, but an isotropic 4D MRI with a high resolution (e.g., $1 \times 1 \times 1\,mm^3$) can also be reconstructed from multiple low-resolution images by using an advanced post-processing method that employs deformable image registration and super-resolution reconstruction [15]. If orthogonal image slices are simultaneously acquired using multiband RF pulses and simultaneous image refocusing [16], the total scan time can be reduced.

The patient 4D MRI often presented very dark liver signals for some patients who received multiple blood transfusions, (Fig. 2C), possibly because of iron overload in the liver, which enhanced the MR relaxation rates [17]. A balanced gradient-echo sequence providing T2/T1 contrast could be an alternative for such cases provided the effect of the inherent banding artifact of that sequence is not severe.

Stitching artifacts were apparent in the 4D MRI for patients showing severe breathing irregularity (Fig. 2B). Incorporating audio coaching or visual-feedback devices [18,19] would reduce breathing irregularity, but children may not always cooperate with these methods. Alternatively, the effect of irregular breathing could be mitigated by a longer calibration period or by reducing the tolerance of triggering amplitude levels with the compromise of a longer scan time. For patients younger than 7 years who exhibit breathing irregularities, the trade-off between longer anesthesia and the accuracy of 4D MRI needs to be evaluated beforehand. However, the scan time is becoming of less concern as the prospective gating method evolves with advanced triggering schemes such as the “efficient solution based on the greedy strategy” (ESGS) [9]. The use of propofol in anesthesia may increase respiratory frequency [20] but might be confounded by patient-specific co-induction opioids that slow respiration [21]. We did not consistently observe the effect of anesthesia for the five patients younger than 7 years.

In conclusion, prospective gating provided a favorable 4D MRI for treatment planning for pediatric and young adult patients. The phantom experiment showed that the prospective gating was superior to retrospective sorting in reducing stitching artifacts. The imaging tended to take longer and to give larger sorting errors with deeper and irregular breathers, who are not uncommon among older children and adolescents. The treatment margins determined by clinical 4D MRI and 4D CT were comparable unless the breathing characteristics changed between the two imaging sessions.

Declaration of Competing Interest

The authors declare the following financial interests/personal relationships which may be considered as potential competing interests: St. Jude Children’s Research Hospital has a research agreement with Philips Healthcare.

Acknowledgements

The authors thank David Sobczak for technical support, Keith A. Laycock, PhD, ELS, for scientific editing, and Lizette Warner, PhD, for facilitating this research. This study was sponsored in part by ALSAC.

Appendix A. Supplementary data

Supplementary data to this article can be found online at https://doi.org/10.1016/j.phro.2019.09.004.

References

[1] Deng Z, Pang J, Yang W, Yue Y, Sharif B, Tuli R, et al. Four-dimensional MRI using three-dimensional radial sampling with respiratory self-gating to characterize temporal phase-resolved respiratory motion in the abdomen. Magn Reson Med 2016;75:1574–85.
[2] Rank CM, Heußsser T, Buzan MT, Wetscherek A, Freitag MT, Dinkel J, et al. 4D respiratory motion-compensated image reconstruction of free-breathing radial MR data with very high undersampling. Magn Reson Med 2017;77:1170–83.
[3] Mickevicius NJ, Paulson ES. Investigation of undersampling and reconstruction algorithm dependence on respiratory correlated 4D-MRI for online MR-guided radiation therapy. Phys Med Biol 2017;62:2910–21.
[4] Han F, Zhou Z, Cao M, Yang Y, Sheng K, Hu P. Respiratory motion-resolved, self-gated 4D-MRI using rotating cartesian k-space (ROCK). Med Phys 2017;44:1359–68.
[5] Hu Y, Caruthers SD, Low DA, Parikh PJ, Mutic S. Respiratory amplitude guided 4-dimensional magnetic resonance imaging. Int J Radiat Oncol Biol Phys 2013;86:198–204.
[6] Du D, Caruthers SD, Glide-Hurst C, Low DA, Li HH, Mutic S, et al. High-quality T2-weighted 4-dimensional magnetic resonance imaging for radiation therapy applications. Int J Radiat Oncol Biol Phys 2015;92:430–7.
[7] Glide-Hurst CK, Kim JP, To D, Hu Y, Kadbi M, Nielsen T, et al. Four dimensional magnetic resonance imaging optimization and implementation for magnetic resonance imaging simulation. Pract Radiat Oncol 2015;5:433–42.
[8] Li G, Wei J, Olek D, Kadbi M, Tyagi N, Zakian K, et al. Direct comparison of respiration-correlated four-dimensional magnetic resonance imaging reconstructed using concurrent internal navigator and external bellows. Int J Radiat Oncol Biol Phys 2017;97:596–605.
[9] Du D, Mutic S, Li HH, Hu Y. An efficient model to guide prospective T2-weighted 4D magnetic resonance imaging acquisition. Med Phys 2018;45:2453–62.
[10] Uh J, Krasin MJ, Li Y, Li X, Tinkle C, Lucas Jr JT, et al. Quantification of pediatric abdominal organ motion with a 4-dimensional magnetic resonance imaging method. Int J Radiat Oncol Biol Phys 2017;99:227–37.
[11] Lu W, Nystrom MM, Parikh PJ, Fooshee DR, Hubenschmidt JP, Bradley JD, et al. A semi-automatic method for peak and valley detection in free-breathing respiratory waveforms. Med Phys 2006;33:3634–6.
[12] Boye D, Lomax T, Knopf A. Mapping motion from 4D-MRI to 3D-CT for use in 4D dose calculations: a technical feasibility study. Med Phys 2013;40:061702.
[13] Tryggestad E, Flammang A, Han-Oh S, Hales R, Herman J, McNutt T, et al. Respiration-based sorting of dynamic MRI to derive representative 4D-MRI for radiotherapy planning. Med Phys 2013;40:051909.
[14] Uh J, Khan MA, Hua C. Four-dimensional MRI using an internal respiratory surrogate derived by dimensionality reduction. Phys Med Biol 2016;61:7812–32.
[15] Freedman JN, Collins DJ, Gurney-Champion OJ, McClelland JR, Nill S, Oelfke U, et al. Super-resolution T2-weighted 4D MRI for image guided radiotherapy. Radiother Oncol 2018;129:486–93.
[16] Mickevicius NJ, Paulson ES. Simultaneous acquisition of orthogonal plane cine imaging and isotropic 4D-MRI using super-resolution. Radiother Oncol 2019;136:121–9.
[17] Queiroz-Andrade M, Blasbalg R, Ortega CD, Rodstein MA, Baroni RH, Rocha MS, et al. MR imaging findings of iron overload. Radiographics 2009;29:1575–89.
[18] To DT, Kim JP, Price RG, Chetty IJ, Glide-Hurst CK. Impact of incorporating visual biofeedback in 4D MRI. J Appl Clin Med Phys 2016;17:128–37.
[19] Lee D, Greer PB, Paganelli C, Ludbrook JJ, Kim T, Keall P. Audiovisual biofeedback improves the correlation between internal/external surrogate motion and lung tumor motion. Med Phys 2018;45:1009–17.
[20] Chidambaran V, Costandi A, D'Mello A. Propofol: a review of its role in pediatric anesthesia and sedation. CNS Drugs 2015;29:543–63.
[21] Mills GH. Respiratory physiology and anaesthesia. Br J Anaesth CEPD Rev 2001;2:35–9.